The paper is published in the Proceedings of SPIE, 1999, **3687**, 205–212.

Molecular Dynamics Investigation of Spall Fracture

A. M. Krivtsov[1], Y. I. Mescheryakov[2]

[1] *St.-Petersburg State Technical University, Department of Theoretical Mechanics, Politechnicheskaya 29, 195251 St.-Petersburg, Russia.*

[2] *Russian Academy of Sciences, Institute for Problems of Mechanical Engineering, V.O. Bolshoj 61, 199178 St.-Petersburg, Russia.*

ABSTRACT

Molecular dynamics investigation of central impact of thin plate impactor to target from the same material is presented. The particles are interpreted as elements of the mesoscopic scale level. Relation of the strain, velocity, and dispersion inside the material on the longitudinal coordinate z is investigated. It is shown that the particle velocity dispersion is initialized by the shock wave front and follows it with a small delay. From the computer experiments it follows that in spite of the double free surface velocity rise the velocity dispersion on the free surface doesn't increase. Kinetic processes in the zone of the spall fracture are investigated.

1. INTRODUCTION

Macroscopic strength characteristics are strongly dependent on the material kinetics in the mesoscopic level (0.1–10 μm). Particles of this scale level (mesoparticles) are formed by dislocation walls, shear bands, rotational cells, and so on. Mesoparticle velocity distribution function and its statistical moments (such as average particle velocity, particle velocity dispersion, excess of the distribution function) can be measured with the interference technique in real time during uniaxial strain shock tests [1, 2]. From the real experiments it is known [2, 3] that the mesoparticle velocity dispersion appears to characterize an ability of material to relax microstresses during the shock wave passage and thereby it defines the macroscopic dynamic strength of the material. But from the experiments it is possible to find out the velocity distribution only on the free surfaces. Information about the velocity distribution inside the material could be obtained only from indirect sources, such as metallographical analysis of the specimens after loading.

That is why we use computer investigations that can help understanding material kinetics inside the specimen during shock loading. Using molecular dynamics simulation we can calculate in the same way the velocity distribution functions inside the material and on its surfaces. If in the areas where we can compare the computer and the experimental investigations they give similar results, then the computer investigation can be used to explore the material behavior in the other areas that are inaccessible in experiments. The mane distinction of the considered method from the classic molecular dynamics is that the particles are interpreted not as atoms or molecules but as elements of the mesoscopic scale level.

2. METHODS

Since the purpose of this study is to understand only the general properties of the mesoparticle velocity distribution functions a simplest molecular dynamics method was used [4, 5, 6]. We have chosen a monoatomic two-dimensional lattice with standard Lennard-Jones 6–12 potential [8]

$$U(r_{ij}) = \epsilon \left[\left(\frac{r_0}{r_{ij}} \right)^{12} - 2 \left(\frac{r_0}{r_{ij}} \right)^{6} \right], \tag{1}$$

where $U(r_{ij})$ is interaction energy between atoms i and j separated by distance r_{ij}, ϵ is the strength of the interaction, and r_0 is a characteristic length scale. Note, that the exact form of the potential is not very important for these investigations [7]. In order to decrease calculation time the potential is usually truncated at a finite distance, beyond which the interaction is taken to be zero. In the considered numeric experiments the cut-off distance was chosen to be $2.1\,r_0$. In this case the interaction potential has contributions from the first, second, and third nearest particles in the perfect crystal. However, the contribution of the second and the third neighbors to the total energy are minimal. Hence, r_0 is approximately the equilibrium, nearest-neighbor atomic separation. In order to describe nonelastic losses of energy small dissipative forces proportional to the particles velocities were added [9]. The simulation technique employed in this work is standard molecular dynamics method [4, 8]: the trajectories of each atom are followed through time by integrating Newton's classical equations of motion. The integration is performed using the method of central differences [8].

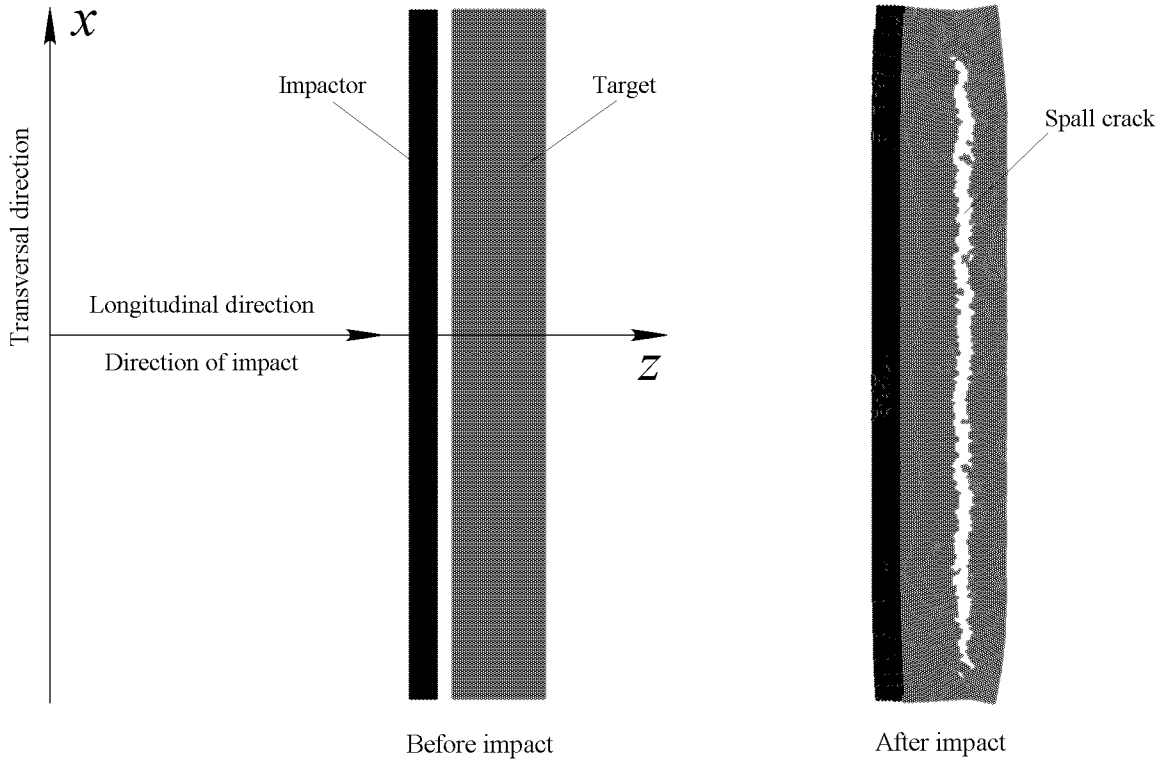

Figure 1: The computation model of the impact loading.

The computation model containing about 20000 particles is presented in the figure 1. The particles are lying in xz plane, z is coordinate in the longitudinal direction (direction of impact), x is coordinate in the transversal direction. The particles are arranged in two rectangles which represent the cross-sections of impactor (black) and target (grey). Initially the particles are arranged on a triangular lattice. The lattice is orientated in such way that one of the sides of the triangles is extended along the x direction. The impactor is placed at an initial distance from the target greater than the cut-off distance of the interparticle potential. Both impactor and target are made from the same particles arranged on the same crystal lattice. Free boundary conditions on all boundaries were used.

Initially the target has zero velocity, impactor has velocity directed along the z axis towards the target. In addition, to initial velocity of each particle a random velocity chosen from a two-dimensional random uniform distribution was added. Let us consider a set of particles indexed by $k = 1, 2, ..., n$. Denote V_{kz}, V_{kx} — projections of the particle velocities to the z and x directions: longitudinal and transversal velocities. Corresponding mean velocities are

$$\overline{V}_z = \frac{1}{n}\sum_{k=1}^{n} V_{kz}\,, \qquad \overline{V}_x = \frac{1}{n}\sum_{k=1}^{n} V_{kx}\,. \tag{2}$$

The dispersions of the longitudinal and transversal velocities are

$$\sigma_z = \frac{1}{n}\sum_{k=1}^{n}(V_{kz} - \overline{V}_z)^2\,, \qquad \sigma_x = \frac{1}{n}\sum_{k=1}^{n}(V_{kz} - \overline{V}_x)^2\,. \tag{3}$$

Further the square root of the dispersions will be used

$$\Delta V_z = \sqrt{\sigma}_z\,, \qquad \Delta V_x = \sqrt{\sigma}_x\,. \tag{4}$$

The quantities ΔV_z, ΔV_x are the mean square deviations of the velocities (further — the deviations) and they have dimension of velocity. Let at the initial moment of time impactor and target have the same initial dispersion $\sigma_{0x} = \sigma_{0y} = \sigma_0$, corresponding to the initial velocity distribution.

3. RESULTS

To make results more visual the scales of time, distance and velocity in the computer experiments are brought similar to the scales in the real experiments with ductile steels [2]. The following sizes were chosen: impactor thickness (z size) is 2 mm, target thickness is 7 mm, impactor width (x size) is 52 mm, target width is same with the impactor width. In figures 4–6 results of the computer experiments are presented. Pattern consists of about 20000 particles. The impactor velocity is 300 m/s.

Rows in figures 5–6 corresponds sequential moments of time after the experiment beginning. Columns in figures 4–5 show dependencies of longitudinal strain, longitudinal velocity V_z, deviation ΔV_z of the longitudinal velocity, and deviation ΔV_x of the transversal velocity on the longitudinal coordinate z. Positive strain values mean compression, negative values mean tension. The coordinate z is coordinate of particles in impactor and target at the moment of time $t = 0$. After the first contact (approximately at $t = 0.05\,\mu$s) the impactor and the target touch along the whole x surface. Thus the first 2 mm the z coordinate correspond to the impactor, the rest 7 mm correspond to the target. For each z value the strain and the longitudinal velocity V_z are averaged over one column of particles (chain of particles extended in the transversal direction). To avoid boundary effects only the central half part of this column is taken. The same set of particle is used to calculate the deviations.

The first row ($t = 0.0\,\mu$s) in figure 4 corresponds to the experiment beginning. The strain (the first graph) is equal to zero except the area on the border between impactor and target. The great negative values in this area correspond to the initial space between impactor and target. The graph for the longitudinal velocity V_z (the second graph in the first row) has a step-like form: $V_z = 200$ mm for the first 2 mm (impactor), and V_z vanishes for the rest area (target). The deviations of the longitudinal and transversal velocities (the 3rd and the 4th graphs) in the considered scale coincide with zero.

The second row ($t = 0.1\,\mu$s) in figure 4 corresponds to the impact beginning. The shock wave of compression is well visible in the first graph, the wave extends from the border between impactor and target symmetrically in two directions: forward (inside the target) and backward (inside the impactor). The second graph shows the well-known theoretical result that the mass velocity in material is twice smaller then the impactor velocity. The three areas with different constant velocity values could be selected in the second graph: the first area with $V_z = 300$ m/s corresponds to the part of the impactor that was not reached yet by the shock wave; the second area with $V_z = 150$ m/s corresponds to the parts of the impactor and the target perturbed by the shock wave; the third area with zero velocity corresponds to the part of the target that was not reached by the shock wave. The deviations (the 3rd and the 4th graphs) are still negligible.

The 4th row ($t = 0.3\,\mu$s) in figure 4 corresponds to the moment of time short after the impact wave has reached the free surface of the impactor. On the first graph we can see a wave of tension, generated by the shock wave reflection from the impactor's free surface. The second graph shows that the mass velocities in the tension area are negative. The 3rd and the 4th graphs in figure 4 show appearance of the velocity dispersion.

The next two rows ($t = 0.4\,\mu$s, $t = 0.5\,\mu$s) show the shock wave propagation inside the target. Consider the 3rd graph in these rows: dependence of the longitudinal velocity deviation ΔV_z on the z coordinate. It is well to see that the deviation appears immediately after the wave front; the deviation grows up to the maximum value that follows the wave front with some delay (about 1.5 mm); after the maximum the deviation slowly decreases to an equilibrium value. Thus the particle velocity dispersion is generated by the front of the shock wave. The 4th graph shows that values of the transversal velocity deviation ΔV_x are close to those of the longitudinal velocity deviation ΔV_z, but the delay after the shock wave front is little bit greater and maximum values of ΔV_x are smaller.

The row $t = 0.7\,\mu$s corresponds to the moment of time short after the impact wave has reached the free surface of the target. On the first graph we can see a wave of tension, generated by the shock wave reflection from the target's free surface. The second graph shows the well known theoretical result of the double increasing of the free surface velocity: the mass velocities grows in two times when the shock wave front reaches the free surface; hence the free surface velocity of the target became equal to the impactor velocity. But an unexpected result is shown in the 3rd and the 4th graphs: the velocity deviations don't increase on the free surface. So the dispersion behavior on the free surface differs much from the velocity behavior.

In the first graph in the row $t = 0.8\,\mu$s (figure 5) it is well to see two waves of tension running towards each other. When the waves mit (row $t = 1.0\,\mu$s) they form an area of very strong tension where little bit later a spall fracture arises (see the narrow area with great negative values in the first graph for $1.2\,\mu\text{s} \le t \le 1.5\,\mu$s). Then wave of tension followed with a little increase of ΔV_z runs in negative direction towards the free surface of the impactor ($t = 1.5\,\mu$s). Now consider the 3rd column: the longitudinal velocity deviation ΔV_z. It is well to see that in the spall zone the deviation has a sharp maximum. The same effect is visible for the transversal velocity deviation ΔV_x, but the maximum values are far smaller (the 4th column).

In the first column for $1.2\,\mu\text{s} \le t \le 1.5\,\mu$s the oscillations in the spall plate are well visible. This oscillations

make the dispersion in the spall plate greater then average dispersion in the rest of the pattern (the 3rd and the 4th columns).

Crack formation in the specimen is shown in figure 6. As it was in figures 5–6, the first column shows longitudinal strain. The second column show the longitudinal velocity deviation ΔV_z. The last column shows the specimen state at the corresponding moments of time. At $t = 0.9\,\mu$s there are now fracture yet. At $t = 1.0\,\mu$s it is possible to see a lot of tiny cracks, which grow at $t = 1.1\,\mu$s, and at $t = 1.2\,\mu$s they join in greater cracks extended in transversal direction. At $1.3\,\mu\text{s} \le t \le 1.5\,\mu$s all existing cracks join in one turnpike crack, and at $t = 1.6\,\mu$s the spall crack formation in the central zone of the target is finished. Note that the width of the spall plate is close to the width of the impactor, how it follows from the theory. From figure 6 it follows that the highest value of the deviation maximum corresponds to $t = 1.3\,\mu$s, when the turnpike crack formation starts. This result is in good agreement with the results obtained in [10].

4. DISCUSSION

In quantities that can be calculated on the base of the continuum mechanics (such as longitudinal strain and mass velocity) the presented computer experiments show a very good agreement with theory: propagation of the shock wave, reflection of the shock wave from the free surfaces, relation between the free surface velocities and velocities inside material, spall formation in the point of two tension waves contact and so on [11]. From the other hand the considered model gives a very good agreement in quantities that could be measured in both computer and real experiments, such as free surface velocity and mesoparticle velocity dispersion on the free surface — see [2, 10, 12]. This gives certainty that the quantities that can't be measured in reality (such as velocity dispersion inside the material) can be estimated from the presented computer experiments. The most unexpected computer result is that the velocity deviations don't increase on the free surface, how it happens with the velocity.

The computer model used to obtain the considered results was very simple: ideal monoatomic lattice with Lennard-Jones potential. If we consider the particles as elements of microscopic scale level (for example, atoms) then the results can be interpreted in the other way: we have investigated spall formation in an ideal monocrystal. In this case instead of the term mesoparticle velocity dispersion we should use term absolute temperature. Of course the considered model is very crude to describe kinetics and dynamic strength properties of real solids, but the general tendencies it should describe properly.

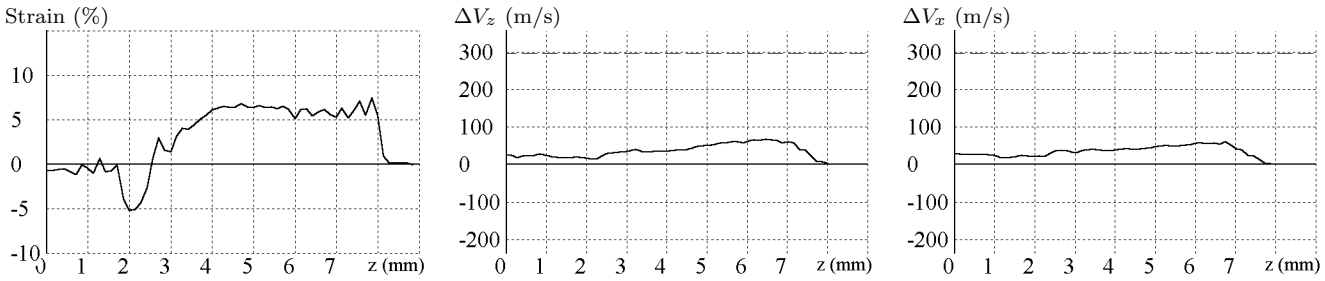

Figure 2: Dispersion is increasing after the wave front ($t = 0.5\,\mu$s).

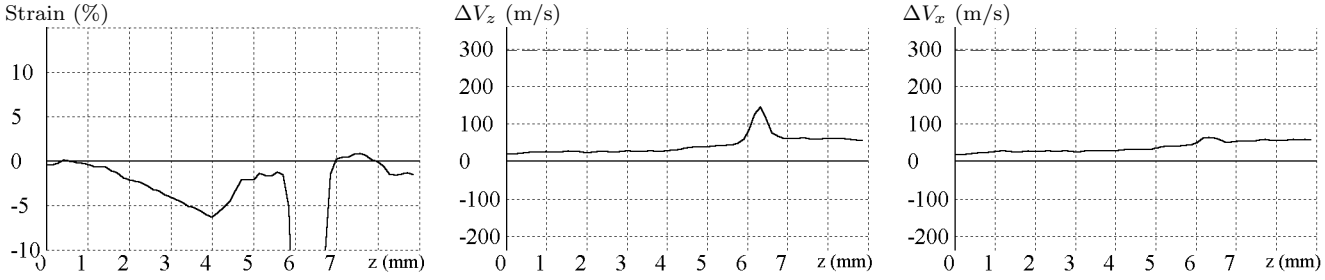

Figure 3: Localized maximum of the dispersion in the spall fracture zone ($t = 1.3\,\mu$s).

5. CONCLUSIONS

- Dispersion of the longitudinal velocity ($\sigma_z = \Delta {V_z}^2$) is initialized by the shock wave front and follows it with a small delay (see figure 2).
- Dispersion of the transversal velocity ($\sigma_x = \Delta {V_x}^2$) is close to σ_z but it follows the shock wave front with larger delay (see figure 2).
- The dispersions have localized maximum in the zone of the spall fracture (in this zone ΔV_z is more then twice greater then ΔV_z in the surrounding area) (figure 3).
- The greatest value of the velocity dispersion in the spall zone realizes at the start moment of the turnpike crack formation.
- Average dispersion in the spall plate is greater then average dispersion in the rest of the pattern (figure 3).
- In spite of the double free surface velocity increase, the velocity dispersion on the free surface doesn't increase.

6. ACKNOWLEDGEMENTS

This work was sponsored by Army Research Laboratory, contract N DAALO1-96-M-0141.

7. REFERENCES

[1] Asay, J. R. and Barker, L. M., "Interatomic measurement of shock-induced internal particle velocity and spatial variation of particle velocity". *J. Appl. Phys.,* 1974, **45**, 2545–2550.

[2] Mescheryakov, Y. I. and Divakov, A. K., "Multiscale kinetics of microstructure and strain-rate dependence of materials". *DYMAT J.,* 1994, **4**, 271–287.

[3] Mescheryakov, Y. I., Mahutov, N. A., and Atroshenko, S. A, "Micromechanisms of dynamic fracture of ductile high-strength steels", *J. Mech. Phys. Sol,* 1994, **42**, 1435–1457.

[4] Allen, M. P. and Tildesley, A. K., *Computer Simulation of Liquids.* Clarendon Press, Oxford, 1987.

[5] Melker A. I., Vorobyeva T. V., "Computer simulation and molecular theory of self-organization and mechanical properties of polymers". *Polymer Engineering and Science*, **36**(2), 162–174 (1996).

[6] Krivtsov, A. M., Zhilin, P. A., Particle Simulation of Large Inelastic Deformations. *Transactions of the 14th Int. Conf. on Structural Mechanics in Reactor technology (SMiRT 14),* 1997, Lyon, France, 121–128.

[7] Michajlin A. I., Melker A. I., "Two-step brake of interatomic bond". *Chemical physics*, **4**, 1, 15–20 (1985).

[8] Eckstein, W., *Computer Simulation of Ion-Solid Interactions.* Springer-Verlag, Berlin, Heidelberg, 1991.

[9] Nagy, I., László, J., and Giber, J., *Z. Phys.,* 1985, **A321**, 221.

[10] Yano, K., Horie, Y., Numerical Computation of Non-equilibrium Particle Velocities within Shock Structure in Condensed Mixtures. *1997 Topical Conference on Shock Compression of Condensed Matter*, 1997, Amherst, MA, USA.

[11] Curran, D. R. and Seaman, L., Dynamic failure of solids. *Phys. Reports,* 1987, **147**, 253–388.

[12] Krivtsov, A. M., Computer Investigation of Relation between Spall Strength and Mesoparticle Velocity Dispersion. *Proc. of the XXV Summer School "Nonlinear Oscillations in Mechanical Systems",* 1998, St.-Petersburg, Russia.

Figure 4: Distribution of strain, velocity and dispersion along the impact direction $(0 < t < 0.7\,\mu s)$.

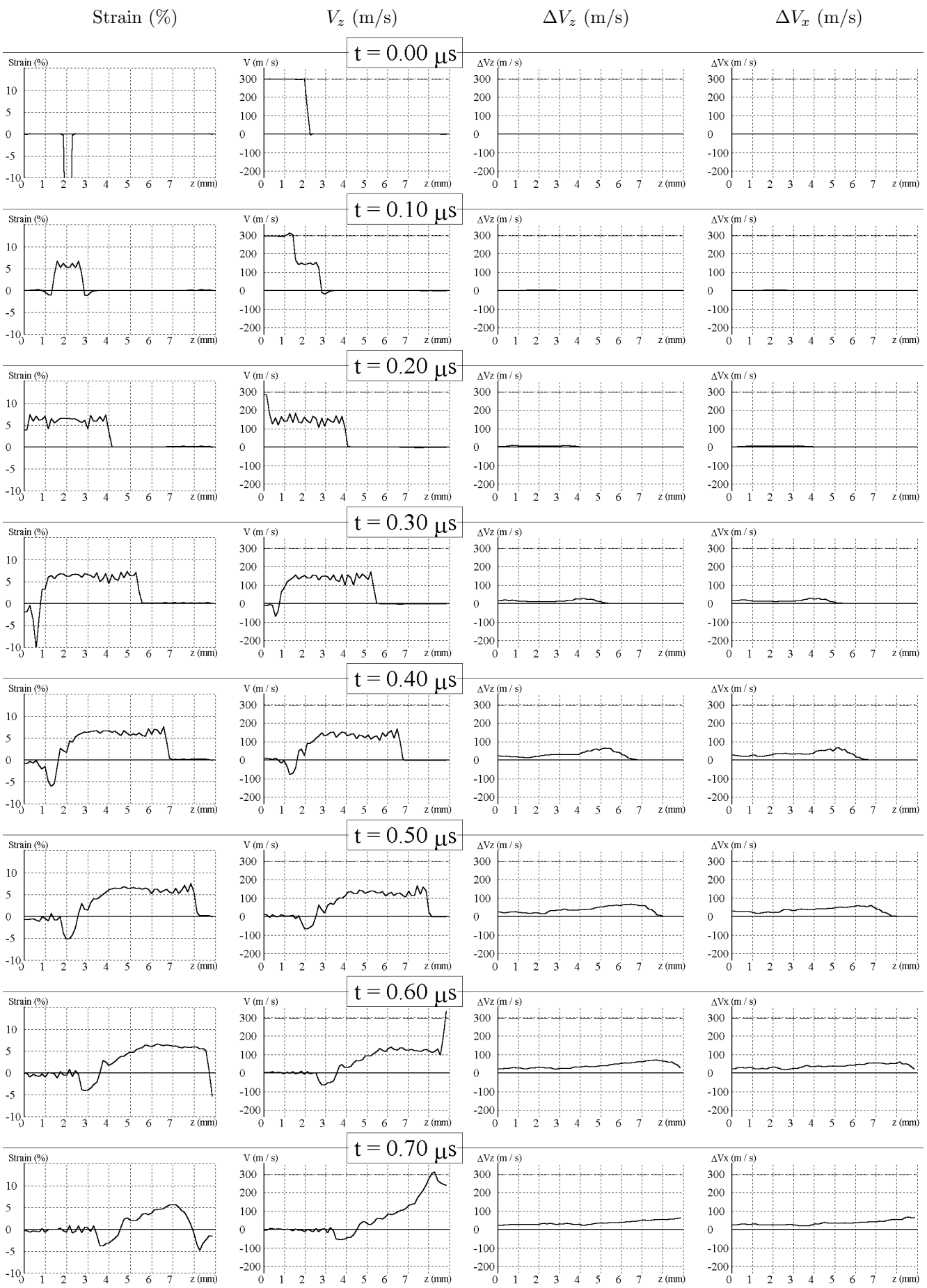

Figure 5: Distribution of strain, velocity and dispersion along the impact direction $(0.7\,\mu s < t < 1.5\,\mu s)$.

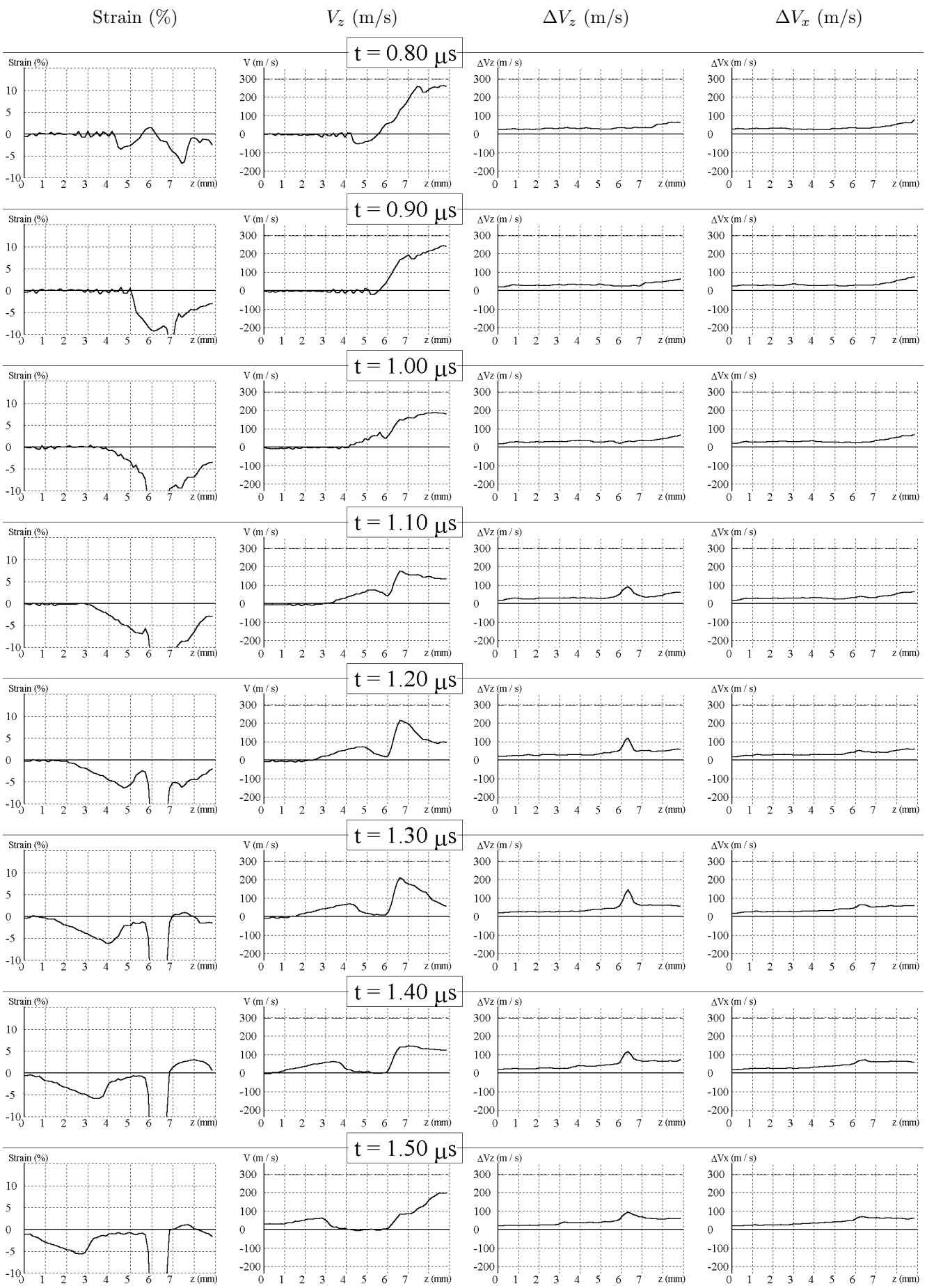

Figure 6: Spall formation in the target ($0.9\,\mu s < t < 1.6\,\mu s$).